The Lazarus project: A pragmatic approach to binary black hole evolutions

John Baker
Albert-Einstein-Institut, Max-Planck-Institut für Gravitationsphysik, Am Mühlenberg 1, D-14476 Golm, Germany and Laboratory for High Energy Astrophysics, NASA Goddard Space Flight Center, Greenbelt, Maryland 20771

Manuela Campanelli
Albert-Einstein-Institut, Max-Planck-Institut für Gravitationsphysik, Am Mühlenberg 1, D-14476 Golm, Germany and Department of Physics and Astronomy, The University of Texas at Brownsville, Brownsville, Texas 78520

Carlos O. Lousto
Albert-Einstein-Institut, Max-Planck-Institut für Gravitationsphysik, Am Mühlenberg 1, D-14476 Golm, Germany; Department of Physics and Astronomy, The University of Texas at Brownsville, Brownsville, Texas 78520; and Instituto de Astronomía y Física del Espacio–CONICET, Buenos Aires, Argentina
(Received 19 April 2001; published 7 January 2002)

We present a detailed description of techniques developed to combine 3D numerical simulations and, subsequently, a single black hole close-limit approximation. This method has made it possible to compute the first complete waveforms covering the post-orbital dynamics of a binary–black-hole system with the numerical simulation covering the essential nonlinear interaction before the close limit becomes applicable for the late time dynamics. In order to couple full numerical and perturbative methods we must address several questions. To determine when close-limit perturbation theory is applicable we apply a combination of invariant *a priori* estimates and *a posteriori* consistency checks of the robustness of our results against exchange of linear and nonlinear treatments near the interface. Our method begins with a specialized application of standard numerical techniques adapted to the presently realistic goal of brief, but accurate simulations. Once the numerically modeled binary system reaches a regime that can be treated as perturbations of the Kerr spacetime, we must approximately relate the numerical coordinates to the perturbative background coordinates. We also perform a rotation of a numerically defined tetrad to asymptotically reproduce the tetrad required in the perturbative treatment. We can then produce numerical Cauchy data for the close-limit evolution in the form of the Weyl scalar ψ_4 and its time derivative $\partial_t \psi_4$ with both objects being first order coordinate and tetrad invariant. The Teukolsky equation in Boyer-Lindquist coordinates is adopted to further continue the evolution. To illustrate the application of these techniques we evolve a single Kerr hole and compute the spurious radiation as a measure of the error of the whole procedure. We also briefly discuss the extension of the project to make use of improved full numerical evolutions and outline the approach to a full understanding of astrophysical black-hole–binary systems which we can now pursue.

DOI: 10.1103/PhysRevD.65.044001 PACS number(s): 04.25.Nx, 04.30.Db, 04.70.Bw

I. INTRODUCTION

Binary–black-hole mergers are among the most powerful and efficient sources of gravitational radiation in our universe and are thus the primary targets for direct experimental detection by the future interferometric observatories. Recent astronomical observations of x-ray emission sources reinforce the evidence of black holes in many galaxies, and astrophysical simulations of globular clusters [1,2] show binary–black-hole mergers in such an abundance as to boost the gravitational wave detection rate estimation to $1.6 \times 10^{-7}\ \mathrm{yr}^{-1}\ \mathrm{Mpc}^{-3}$, which results in about one detection event every 2 years for the Laser Interferometric Gravitational Wave Observatory (LIGO) and in one event per day for LIGO II.

It is thus not surprising that on the theoretical side the study of binary–black-hole mergers has become one of the most exciting and challenging topics in astrophysical relativity. Several theoretical approaches have been developed for treating these systems. So far the post-Newtonian (PN) approximation has provided a good understanding of the early slow adiabatic inspiral, or ''far-limit,'' phase of these systems. Similarly, for the final moments, when black holes are close enough to each other to sit inside a common gravitational well, one can successfully apply the ''close limit'' (CL) approximation [3], which effectively describes the whole system as a perturbation of a single black hole which rapidly ''rings down'' to stationarity. Before this last stage, though, when the black holes are still close to the *innermost stable circular orbit* (ISCO), the orbital dynamics are expected to yield to plunge and coalescence. No approximation method can be applied in this highly nonlinear phase and it is generally expected that one can treat the system only by a full numerical (FN) integration of Einstein's equations.

Intensive efforts have been under way in the past decade to develop numerical codes able to solve Einstein's general relativity equations, by the use of powerful supercomputers. So far the numerical treatment of black hole systems in full three dimensions (3D) has proved very difficult and challenging because of the huge computer memory requirements, on one hand, and very severe numerical instabilities, on the other, which make the codes fail before any useful gravita-

tional wave information can be extracted. In spite of such difficulties, interesting progress has been made, including, for example, the work in [4], where a true 3D simulation based on the traditional $3+1$ decomposition of space and time has been successfully carried out for the so-called nonaxisymmetric ''grazing'' collisions of two black holes. However, because of the limited evolution time achievable before these codes become unstable or otherwise inaccurate these simulations must still begin too late in the plunge to be practical for direct astrophysical application. In most cases treatable so far, the close limit approximation theory represents a good alternative model for the late time dynamics of these systems.

Considering the above situation, in Refs. [5,6] we introduced a new hybrid approach to the binary–black-hole merger problem, called the *Lazarus project*, with the motivation of providing expectant gravitational wave observers with some early estimate of the full merger waveforms within a ''factor two,'' and to guide future, more advanced numerical simulations. The key idea of the Lazarus project is very simple: combine the best of the already existing approaches by applying each of these methods in sequence and in their best suited regime, while focusing the numerical simulations squarely on the intermediate phase of the interaction where no available perturbative approach is applicable.

Clearly, the primary task of the combined model is developing appropriate interfaces between these three existing treatments in such a way that we can also benefit from future improvements in any of the above three approaches. In an earlier Letter [5] we presented the first results of our eclectic approach for a model problem, the head-on collision of black holes, where we successfully addressed the problem of combining the close-limit approximation describing ringing black holes and full three-dimensional numerical relativity. In this well-known case, our method proved capable of determining radiation waveforms with accuracy comparable to the best published 2D numerical results, allowing at the same time a more direct physical understanding of the collisions and indicating clearly when nonlinear dynamics are important as the final black hole is formed. Previous attempts to make a combined use of numerical and close-limit evolution [7] have been implemented in the case of two axisymmetric black holes formed by collapsing matter [8], using a 2D numerical code and $l=2$ metric perturbations (in the manner of Zerilli) of the Schwarzschild background and are not generalizable to full 3D simulations. In Ref. [6] we studied the nonaxisymmetric coalescence of equal mass nonspinning binary black holes from an estimate of the innermost stable circular orbit down to the final single rotating black hole, and provided the first, astrophysically plausible, theoretical predictions for the gravitational radiated energy, angular momentum, and waveforms to be expected from these systems.

A sketch of the eclectic approach to the binary black hole calculation is outlined in the following steps: (1) First provide a description of the early dynamics of the system with an approach, such as the post-Newtonian method, which is appropriate for slowly moving, well-separated black holes. A recent interest within the post-Newtonian and gravitational wave research community in providing Cauchy data for simulations may soon lead to a practical PN-FN interface. (2) Extract critical information about the late-time configuration of this system, and translate this information to a corresponding solution of the gravitational initial-value problem. (3) Apply a full 3D numerical simulation of Einstein's equations to generate a numerical spacetime covering the nonlinear interaction region of the spacetime. The evolution should proceed for long enough so that the subsequent evolution of the region exterior to the final single remnant black hole can be well approximated by perturbative dynamics. (4) At this point choose a ''late-time'' slice from the numerically generated spacetime and extract $\psi_4=C_{\alpha\beta\gamma\delta}n^\alpha\bar{m}^\beta n^\gamma\bar{m}^\delta$ and $\partial_t\psi_4$, to quantify the deviation of the numerical spacetime from a Kerr geometry. Then (5) evolve via the Teukolsky equation, which governs the dynamics of Kerr perturbations in the time domain [9], long enough to drive all significant radiation into the radiation zone where it can be interpreted. Making the greatest possible use of perturbation theory in this way not only saves precious three dimensional computational resources, concentrating these, for the first time, squarely in the intermediate coalescence phase, but also provides a new framework to explore and interpret the interesting new physics that is expected to take place in the transition from nonlinear to linear dynamics.

The emphasis of this paper is to realize steps 2–5 above and to describe in detail a general approach to providing the FN-CL interface. In Sec. II we discuss our approach to the full numerical simulations which we have used to achieve a successful evolution of truly detached black holes for the first time. This discussion naturally divides into two parts: (a) our preparation of the initial data, by which we greatly improve the simulation efficiency and (b) our numerical evolution method.

Two important questions arise in implementing the transition, step 3, from a numerical approach to a perturbative approach. First, how long must we evolve the system numerically before we can obtain a reliable description in terms of a single perturbed black hole? We use a combination of several independent and complementary indicators to establish when perturbation theory should begin to work. In Sec. III, we discuss our study of two of such indicators: (a) The speciality invariant, $\mathcal{S}$, introduced in Ref. [10], which is exactly equal to 1 for the Kerr geometry with leading deviations quadratic in the gravitational distortions; (b) Cauchy data extracted at successively later numerical time slices. When the system has entered the linear regime, the waveforms evolved via the Teukolsky equation should essentially superpose on each other. Consequently also a certain leveling off of the radiated energy should be observed. While (a) gives a local measure of the physical distortions from the Kerr geometry, (b) rather depends on the past light cone data.

The second question is how to identify the single ''background'' black hole that is emerging in the numerical spacetime. In order to define deviations from this background black hole we must be able to relate it, by an explicit diffeomorphism, to the numerical spacetime. We need to specify both the spatial coordinates and the time slice, which in general may be different from the one used to numerically inte-

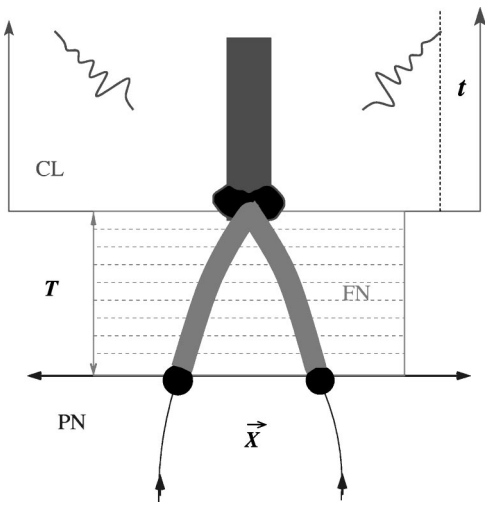

FIG. 1. The eclectic approach: We represent the three phases of the binary–black-hole evolution and the corresponding techniques adapted to each phase. The full numerical evolution is located to cover the truly nonlinear dynamical interaction. The domain of perturbative evolution (CL) follows the FN domain allowing indefinite evolution. Waveforms are extracted at the dotted world line depicted on the right. Though such observers are located in the CL part of the spacetime they will experience all radiation arriving from the strong field dynamical FN region. In the far limit regime we envision using the post-Newtonian approximation

grate the Einstein equations. This geometrical puzzle is discussed in detail in Sec. IV. There is in general no geometrically preferred way to associate the numerical and background spacetimes, but the first order gauge and tetrad invariance of the perturbative formalism implies that the results should not depend strongly on small variations in these choices.

In Sec. V, we describe how to compute the Cauchy data for the Teukolsky equation, i.e. the Weyl scalar ψ_4 and its background time derivative $\partial_t\psi_4$, from the numerical three-metric g_{ij} and extrinsic curvature K_{ij}, on the transition Cauchy hypersurface. The numerical calculation of the Cauchy data requires, first, a nontrivial identification of an appropriate numerical ''tetrad,'' which reduces to the (null and complex) tetrad used in the perturbative calculation in the small perturbation limit. Second, the numerical calculation of $\partial_t\psi_4$ is done ''on slice'' using Einstein's equations to be consistent with the Boyer-Lindquist time of the final Kerr black hole.

In Sec. VI we briefly describe the perturbative Teukolsky equation and the $2+1$ numerical code used to solve it numerically. We then apply all of our techniques, in Sec. VII, to evolution of a single Kerr black hole with vanishing shift and maximal slicing to test the consistency of our method (see Fig. 1). Our essentially trivial result is obtained in a very nontrivial way since our numerical tetrad is not necessarily aligned with the principal null directions, nor are our numerical coordinates the Boyer-Lindquist coordinates used in the perturbative code. Only after we make the appropriate rotation of the tetrad and transform the coordinates to reproduce the Boyer-Lindquist ones do we see quadratic convergence to near vanishing outgoing gravitational radiation.

II. SUMMARY OF THE FULL NUMERICAL TECHNIQUES

In our full numerical simulations we use many of the standard techniques applied in, for example, the Binary–Black-Hole Grand Challenge effort, with adaptations appropriate to the needs of our more specifically defined numerical simulation problem. Many previous applications of numerical relativity to the binary–black-hole problem have been developmental test problems aiming toward an ultimate goal of indefinitely long-running 3D numerical simulations to cover the evolution beginning with well separated black holes and evolving through the entire interaction until further radiation is no longer significant. With regard to gravitational radiation, these efforts have been focused on indefinite numerical stability and successful radiation waveform extraction by an observer in the ''faraway'' region of the numerical domain. These efforts have often been successful with relatively brief black hole evolutions, but have demonstrated the serious difficulties in succeeding with the desired long-running numerical simulations, and this approach has not yet generated radiation studies that approach relevance to astrophysical problems.

We will ask less of our numerical simulations. Our demand is for a highly accurate determination of the most significantly nonlinear part of the binary interaction. We will try to make use of codes that may only run stably for a relatively brief period, but which can provide an accurate representation of the part of the spacetime we are most interested in. This point of view allows us, for example, to avoid the difficult problem of imposing physically accurate outer boundary conditions, by considering only the part of the spacetime causally separated from the boundary. We find that this can be done much more efficiently in specialized coordinates, described in the first section below. Similarly, we have not yet needed more stable formulations of Einstein's equations, or difficult sophisticated techniques such as black hole excision. Our straightforward numerical approach to evolution is described in the second section.

A. Preparing the initial data

Ultimately we wish to derive initial data based on information from an approximation procedure, such as the post-Newtonian method which is applicable in the limit of slow-moving and far-apart black holes. As no such interface is presently available we use, in our present work, initial data from an alternative source, commonly applied in numerical relativity, the ''puncture'' formalism with conformally flat three-metric and purely longitudinal extrinsic curvature on a maximal slice. This assumes a three-sheeted topology instead of an inversion symmetry across the throats [11], allowing for a solution of the elliptic Hamiltonian constraint equation without having to impose interior boundary conditions [12].

Within this family it is possible to identify data roughly corresponding to quasicircular orbits using the effective potential method as in Ref. [11]. The binding energy of the system is computed as a function of the proper separation of the holes keeping everything else constant. A minimum in the binding energy is then interpreted as giving a stable quasicircular orbit. Within this approach an ISCO is determined

by varying the orbital angular momentum of the system until this minimum becomes an inflection point. For less separated configurations, a stable quasicircular orbit is no longer possible. We use these ISCO data, determined in [13], for nonspinning equal-mass black holes as a particularly reasonable starting point for approaching astrophysical systems [6].

Having selected the physical initial data we then prepare them for numerical evolution. When Smarr and York [14] spelled out the problem of $3+1$ numerical relativity in the 1970s, they specifically sought out methods that would be invariant to gauge transformations in the initial data. In the pursuit of long-running all-purpose numerical relativity tools, this viewpoint has been traditionally preserved, and little attention has been given to the question of choosing appropriate coordinates for the initial data. It is clear though that, whenever differential equations are to be solved numerically, some choices of variables (coordinates) will be more practical than others. In a wave-propagation problem, for instance, the simulation will be much more efficient if a wave is evenly resolved as it moves across the numerical domain, or similarly if the coordinate characteristic speeds are constant in space and time.

For numerical relativity simulations in practice we are often very far from this ideal. In typical coordinates, such as isotropic coordinates for our (initially) conformally flat spaces, the waves are strongly redshifted as they move away from the strong-field region. Since we require both a physically large computational domain and also high resolution in the strong field region, use of the standard coordinates leads to a great waste of numerical effort on overresolving an outgoing radiation wave that was originally generated with much poorer resolution. In this way, relatively little is gained by expanding the computational domain with additional numerical grid points. We find that we can make great improvements in numerical efficiency with a relatively simple *ad hoc* coordinate transformation on the initial data which we call ''fish-eye'' coordinates. A typical such transformation is a radial rescaling, $r_{iso}=R_{num}\cosh[(R_{num}/R_0)^n]$ with typical values $R_0=7.7$ and $n=2$. This allows us to maintain a central resolution of up to $M/24$ with outer boundaries near $r_{new}=37M$ using only 256×512^2 grid points, moving the outer boundary much farther away without loss of physical resolution in the strong field region. This problem is illustrated in Fig. 2, which shows data from numerical simulations in two alternative coordinate systems after $10M$ of evolution from an initial ISCO configuration. The outgoing radiation wave is noticeable in the real part of the gauge independent $\mathcal{S}$ invariant discussed in Sec. III A. These curves represent the same physical spacetime as seen from alternative numerical coordinate systems. In this figure the strong field dynamics are most important in the left side on the figure up to about the value of the numerical coordinate (along the z axis) of $Z_{num}=6$. Up to that point the two coordinate systems are nearly identical. As we add grid points on the right side of the figure beyond this strong field region, we are frustrated in the isotropic coordinate case by the redshift effect, and only a modest additional part of the outgoing wave, about half a wave cycle, is added to the grid when we roughly triple the grid dimension. In the case of our fish-eye

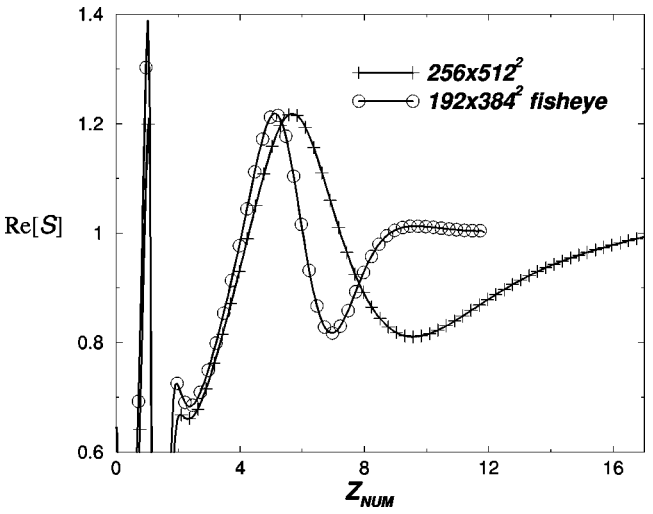

FIG. 2. The benefit of our fish-eye coordinates compared against the typical isotropic coordinates. The S invariant, plotted here, gives an indication of the radiation moving out from an initial ISCO system after $10M$ of numerical evolution. In the strong field region up to $z=6$ the two coordinate systems are very similar. On moving outside that region though, the fish-eye coordinates cover a significantly larger region of the physical spacetime with fewer grid points. The extra grid points in isotropic coordinates are wasted by overresolving the outer part of the radiation. In fish-eye coordinates the wave is resolved more evenly.

coordinate the wave is evidently more evenly resolved across the grid, and we cover the domain of the isotropic coordinate system with only about a 60% increase in the grid dimension. As shown, the fish-eye coordinate system has a much more distant *physical* outer boundary than that of the isotropic case while still having only about half of the grid points in 3D. Note that we would gain no further advantage by attempting to compactify spatial infinity as in for example [15] since the resolution must nevertheless still fail to resolve waves at a finite radius in such a scheme.

Foreseeing longer term full numerical evolutions, we have also implemented other recoordinizations of the initial data that have a fairly constant high resolution in the center of the grid (where the grid stretching is more severe) and a lower resolution near the boundaries, but still fairly constant to allow the application of the usual radiative boundary conditions (adapted to the different characteristic speed). One of these functions is

$$r_{iso}=R_{num}\left\{1+b\left[\tanh\left(\frac{2(R_{num}-R_0)}{d}+0.35\right)+\tanh\left(\frac{2R_0}{d}-0.35\right)\right]\right\}^2 \tag{2.1}$$

with b,d,R_0 adjustable parameters that determine the ratio of central to boundary resolutions and the width and location of the effective resolution transition region, respectively.

B. Numerical evolution

Our numerical evolution must be consistent with our need for highly accurate relatively brief simulations. Conse-

quently, in our work so far, we have used the standard ADM (Arnowitt-Deser-Misner) formulation of the Einstein equations [16] as adapted by Smarr and York [14]. Our evolution equations are thus simply

$$\hat{\partial}_0 g_{ab} = -2\alpha K_{ab}, \tag{2.2}$$

$$\hat{\partial}_0 K_{ab} = -\nabla_a \nabla_b \alpha + \alpha(R_{ab} - 2K_{ac}K^c_b + K_{ab}K) \tag{2.3}$$

where $\hat{\partial}_0 = \partial_t - \pounds_\beta$. Here and below latin indices run from 1 to 3.

Although a newer conformal formulation of Einstein's equations has been found to be more stable in various numerical simulations [17], here we focus on the accuracy of the solutions rather than long term stability. Our observation is that the standard ADM equations seem to give more accurate results for binary black hole simulations in our gauge while the simulation is stable.

If it is possible to have a slicing that is consistent with that of our perturbation theory, then we can avoid the rather large technical problem of producing data on a slice inconsistent with the background. Consistent with our choice of Boyer-Lindquist coordinates in our perturbation treatment of the background black hole, we have chosen maximal slicing to define the lapse α,

$$K = 0, \quad \Delta\alpha = \alpha K_{ab}K^{ab}. \tag{2.4}$$

This implies an elliptic equation for α which we have typically solved every 5 time steps using Dirichlet boundary conditions. For simplicity we set the shift $\beta^i = 0$, which is an adequate condition for relatively brief runs. The numerical evolution is performed using an iterative Crank-Nicholson method of third order which is second order convergent. In our simulations we have used resolutions up to $dx = M/24$ with $dt = 0.25dx$. Because we have moved the outer boundary to a point causally separated from the region we are interested in, it is acceptable simply to impose static boundary conditions.

In evaluating the results of our numerical simulations we make frequent use of two indicators: The degree of satisfaction of the ADM constraint equations gives a measure of the numerical error produced by the evolution

$$\nabla^a(K_{ab} - g_{ab}K) = 0, \tag{2.5}$$

$$R - 2K_{ab}K^{ab} + K^2 = 0. \tag{2.6}$$

These quantities provide an important indication of when numerical inaccuracies (and eventually instabilities) have become significant in our simulations. Even if Einstein's equations could be solved perfectly, any simulation with a finite boundary is subject to an additional type of error arising from inappropriate boundary conditions. A geometrically correct solution may have physically unreasonable disturbances propagating in from the boundary. We have found the speciality invariant S [10] to be a sensitive indicator of such boundary waves, which do not violate the constraints.

III. DETERMINING THE LINEAR REGIME

Black hole perturbation theory has recently generated much interest as a model for the late stages of a binary–black-hole collision spacetime [3]. When two black holes are close enough to each other one can simply treat the problem, in the close limit approximation, as a single distorted black hole that rings down into its final equilibrium state. So after some nonlinear numerical evolution of the full Einstein's equations for a system of two initially well-detached black holes, there should always be a transition time, T, after which the system simply behaves linearly i.e. satisfies the linear perturbation equations around the final Kerr black hole. Finding the *linearization time* T is thus the first nontrivial question that arises in the context of our eclectic approach. In other words, we need one or more working criteria for *when* we can expect perturbation theory to be accurately effective based only on numerical data. As we shall see below, we apply at least two independent criteria for estimating the onset of linear dynamics, the speciality invariant prediction based only on the Cauchy data and another estimate based on the stability of the radiation waveform phase.

A. The speciality invariant test

Motivated by this purpose in Ref. [10] we introduced an invariant quantity,

$$\mathcal{S} = 27\mathcal{J}^2/\mathcal{I}^3, \tag{3.1}$$

where $\mathcal{I}$ and $\mathcal{J}$ are the two complex curvature invariants $\mathcal{I}$ and $\mathcal{J}$, which are essentially the square and cube of the self-dual part, $\tilde{C}_{\alpha\beta\gamma\delta} = C_{\alpha\beta\gamma\delta} + (i/2)\epsilon_{abmn}C^{mn}_{cd}$, of the Weyl tensor:

$$\mathcal{I} = \tilde{C}_{\alpha\beta\gamma\delta}\tilde{C}^{\alpha\beta\gamma\delta} \quad \text{and} \quad \mathcal{J} = \tilde{C}_{\alpha\beta\gamma\delta}\tilde{C}^{\gamma\delta}_{\mu\nu}\tilde{C}^{\mu\nu\alpha\beta}. \tag{3.2}$$

Both these scalars can be expressed in terms of the Weyl components, for an arbitrary tetrad choice:

$$\mathcal{I} = 3\psi_2^2 - 4\psi_1\psi_3 + \psi_4\psi_0,$$

$$\mathcal{J} = -\psi_2^3 + \psi_0\psi_4\psi_2 + 2\psi_1\psi_3\psi_2 - \psi_4\psi_1^2 - \psi_0\psi_3^2. \tag{3.3}$$

The geometrical significance of $\mathcal{S}$ is that it measures the deviations from algebraic speciality (in the Petrov classification of the Weyl tensor).

For the unperturbed algebraically special (Petrov type D) Kerr background $\mathcal{S} = 1$. However, for interesting spacetimes involving nontrivial dynamics, like distorted black holes, which are in general not algebraically special (Petrov type I), we expect $\mathcal{S} = 1 + \Delta\mathcal{S}$, and the size of the deviation $\Delta\mathcal{S} \neq 0$ can be used as a guide to predict the applicability of black hole perturbation theory. In particular we adopt the criterion that, when $\mathcal{S}$ differs from its background value of unity by less than a factor of 2 outside the (background) horizon, a perturbative treatment may be expected to provide a reasonable description of the radiative dynamics. A larger deviation from algebraic speciality implies significant second order

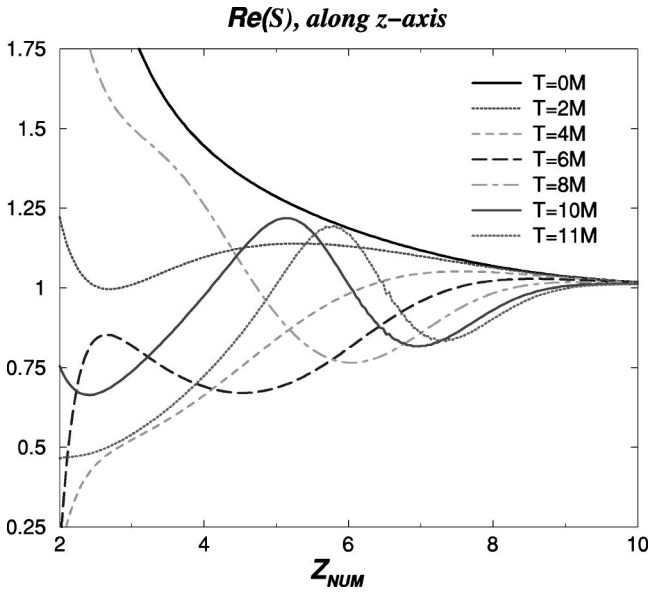

FIG. 3. The speciality invariant for binary black holes evolving from the ISCO showing damped oscillations around unity, its Kerr value. The location of the horizon in these coordinates is roughly 2.5. Its behavior at larger radius suggests that radiation is beginning to leave the system.

perturbations. In fact, for perturbations on a background Kerr spacetime, with an arbitrary tetrad perturbation, one can easily deduce that

$$\mathcal{S}=1-3\epsilon^2\frac{\psi_0^{(1)}\psi_4^{(1)}}{(\psi_2^{(0)})^2}+\mathcal{O}(\epsilon^3), \tag{3.4}$$

where ψ_0, ψ_4 and ψ_2 are the usual Newman-Penrose complex Weyl scalars. The lowest order term in the deviation is second order in the perturbation parameter ϵ, and should tend to vanish if first order perturbation theory is appropriate. Note that the superscripts (0) and (1) stand respectively for background and first order pieces of a perturbed quantity, where ϵ is a perturbation parameter.

In Fig. 3 we display the speciality invariant along the z axis, perpendicular to the orbital plane of two black holes starting the evolution from the ISCO determination used in [6]. Its value oscillates around 1 (the Kerr background value). After some evolution $T\approx 11M$, the amplitude of the oscillation decreases to a deviation below 50% outside the horizon (located at around $Z_{num}\approx 2.5$ in the numerical coordinates), and perturbation theory can reliably take over the remaining of the evolution. Because the gravitational field has two degrees of freedom is it clear that the $\mathcal{S}$ invariant alone is insufficient to provide a complete description of black hole perturbations, and can be complemented with its time variation $\dot{\mathcal{S}}$. Consequently, we have been looking at the turning points where $\dot{\mathcal{S}}=0$ and the amplitude of the distortion reaches a maximum.

As noted in Sec. III, $\mathcal{S}$ is also very useful outside the perturbative context. Its usefulness is derived from the fact that it is a gauge invariant quantity which, unlike I and J, is not dominated by strong ''peeling'' property fall-off behavior, which tends to indicate spacetime dynamics. Because the Weyl tensor, $C_{\alpha\beta\gamma\delta}$, carries information about the gravitational fields in the spacetime, $\mathcal{S}$ turns out to be an interesting indicator of radiation of the spacetime and tests, for instance, how much radiation is produced by the imposition of approximate boundary conditions. We have found that the $\mathcal{S}$ invariant is simple to calculate and can be applied directly to full 3D numerical evolutions to provide a gauge invariant indication of the dynamics.

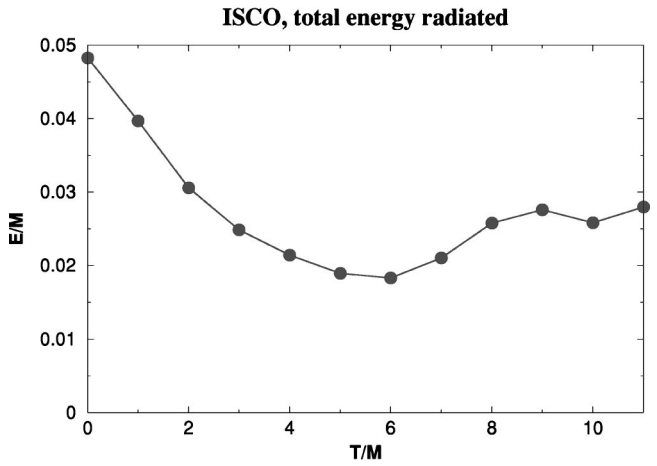

FIG. 4. Energy radiated from two black holes from an ISCO configuration for different transition times showing a plateau when reaching the linear regime.

B. Waveform locking and energy plateau

The phase and the amplitude of the radiation, or equivalently the locking of the waveforms and the corresponding energy plateau, also provide an indicator of linear dynamics. Starting with detached black holes, we expect an initial period of weak bremsstrahlung radiation followed by the appearance of quasinormal ringing. On the other hand, switching to perturbative evolution immediate leads to premature ringing. Hence if we cut short the numerical simulation and apply linear theory too early, we observe quasinormal ringing too early and calculate a waveform that is out of phase with the desired result. Comparing waveforms derived from differing durations of numerical simulation then we tend to see a phase shift in the onset of the ringing when we have not yet allowed enough numerical simulation. In practice, we thus follow the behavior of the waveforms through the evolution by extracting the Cauchy data at successively later numerical time slices. When the system enters the linear regime, the waveforms evolved via the perturbative Teukolsky equation should essentially superpose on each other, as changing this transition time amounts to an equivalent exchange of linear and nonlinear evolution for the intervening region of spacetime. Consequently also a certain leveling off of the radiated energy should be observed (see Fig. 4).

As we show in Fig. 5, extracting waveforms every $1M$ of nonlinear numerical evolution allows us to study the transition to linear dynamics, and to perform important consistency tests on our results. If we have made a good definition

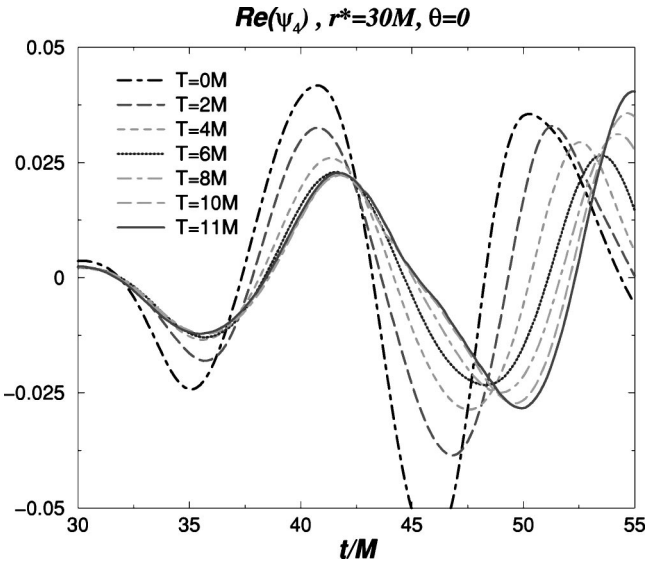

FIG. 5. Detail of the progressive waveform locking process for black holes at the location of the ISCO.

of the perturbative background, as described in Sec. IV, then we can expect our radiation waveform results to be independent of the transition time, T, once the linear regime is reached and for as long as the numerical simulation continues to be accurate.

A closer look at Fig. 5 gives us an idea of how the linearization happens. Curves of $T=10M$ and $11M$ of evolution are close to the correct waveform for this orbital case starting at a proper separation $L/M=4.9$. If we apply right away the close limit approximation we get the curve labeled by $T=0M$ which starts ringing prematurely. After $2M$ of full numerical evolution we obtain good agreement with the correct waveform up to $t/M\approx 33$. When perturbation theory takes over after $4M$ of full numerical evolution the agreement is very good up to $t/M\approx 38$. Near $t/M=45M$ we see that we need $8M$ of nonlinear evolution while near $t/M=50M$ $10M$ of full numerical evolution are needed and at longer times the agreement begins to be fine for the whole relevant waveform. This process shows how the full nonlinear dynamics shifts to a central region covered by the common potential barrier allowing us to describe linearly the evolution of the outer part.

C. Common horizon

An intuitive picture to visualize the applicability of the close limit approximation would be the appearance of a common event horizon that encompasses the binary system. Under these conditions the spacetime exterior to the horizon (the relevant one for computing gravitational radiation reaching infinity) can be treated as perturbations of a Kerr hole. In practice *event* horizons are difficult to compute in numerical relativity because they are a global feature of the spacetime and we would need to first evolve the binary system for a long time and then extract a *posteriori* the information to locate the event horizon. An easier quantity to compute is the *apparent* horizon, which can be defined locally as the outermost marginally trapped surface of the spacetime where a congruence of null rays directed outward have vanishing expansion [18]. A common apparent horizon lies inside and in a binary system appears later than a common event horizon; and typically much later than the time when the system can be effectively described by linear perturbations. The linearization time refers to when the close limit approximation can be applied and this intuitively occurs when a common potential barrier covers the binary system. In black hole perturbation theory, a potential is present somewhat outside the horizon of the black hole which tends to prevent radiation from escaping this region. This is the main reason why the close limit is such a good approximation even beyond the original expectations [19].

IV. CONSTRUCTING THE KERR BACKGROUND

Einstein's theory of gravity in principle demands the equivalence of all coordinate representations of gravitational dynamics. However, in practice one always needs to choose a convenient gauge to accurately carry over the full numerical evolution to the point where the two black hole system effectively behaves like a single perturbed black hole. Having determined that a late time numerical spacetime geometry is close to the Kerr spacetime does not give us any information about the coordinate system in which this is written. In order to be able to continue the numerical evolution with the Teukolsky equation (6.2), we thus need to reconstruct a Kerr background in a recognizable form, for instance in Boyer-Lindquist coordinates. Because there is in general no unique procedure to reconstruct such a Kerr background, we shall require that this should be *close* enough to the given numerical spacetime. In other words, we will require that the two spacetimes agree *to the first order* in ϵ. Since the physics of our problem will then be described by quantities, like ψ_4, which are first order gauge (and tetrad) invariant, the physical results we compute will be independent (to first order) of the identification of the background coordinates we describe below. To have complete theoretical control of the perturbation theory, it is desirable to have a complete family of initial data sets which reduces to the background geometry in the limit $\epsilon\rightarrow 0$. While this requirement is not strictly required in a practical perturbative application [7], we would like to stay as close as possible to this arrangement for its benefit in evaluating our results. In our case the perturbation parameter ϵ can be regarded as a decreasing function of the transition time T. In practice, we will not be able to achieve an exact Kerr black hole in the $T\rightarrow\infty$ limit, but we will aim for the practical goal that the remaining perturbations are small compared to the radiation we are interested in, a condition that we test in Sec. VII.

We initially suppose that the background Kerr black hole is given by the parameters M and a of the initial data. With a first estimate of the total radiated energy and angular momentum these parameters can be iterated to approach the final values for the stationary Kerr black hole.

The Kerr metric in Boyer-Lindquist coordinates (t,r,θ,ϕ) reads

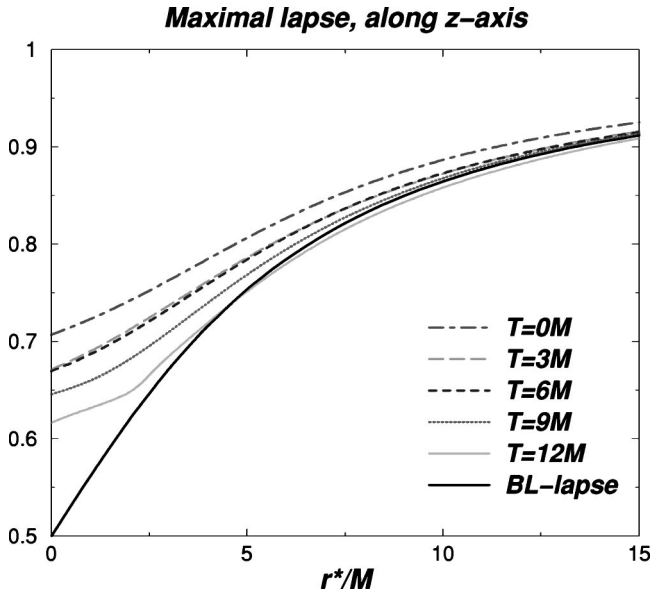

FIG. 6. The maximal lapse used for black holes evolving from the ISCO compared to the analytic Kerr lapse in Boyer-Lindquist coordinates for different evolution times.

$$ds^2 = -\left(1 - \frac{2Mr}{\Sigma}\right)dt^2 + \left(\frac{\Sigma}{\Delta}\right)dr^2 + \Sigma\, d\theta^2 + \sin^2\theta \frac{\Omega}{\Sigma} d\phi^2 - \frac{4aMr}{\Sigma}\sin^2\theta dt d\phi, \tag{4.1}$$

where $\Delta = r^2 - 2Mr + a^2$, $\Sigma = r^2 + a^2\cos^2\theta$ and $\Omega = (r^2 + a^2)\Sigma + 2Mra^2\sin^2\theta$, M is the mass of the black hole, and a its angular momentum per unit mass.

A. The slice

We recall that a Boyer-Lindquist slice of the Kerr metric has $K=0$. The full numerical coordinate condition of maximal slicing, Eq. (2.4), is solved for the lapse α with an exterior boundary condition set to reproduce the value of the Boyer-Lindquist lapse there, but to vanish at the location of the individual black hole ''punctures.'' The resulting lapse from the evolution of two holes from the ISCO is shown in Fig. 6. The lapse resembles the Boyer-Lindquist lapse initially and further evolution brings them closer. Thus the maximal lapse with our boundary condition approaches the background lapse quite closely. Where there are differences, near the horizon, our lapse tends to produce a coordinate system in which the coordinate observers drift slowly into the black hole. Considering our coordinate trajectories from the frame of the background black hole, one can conclude that, since the trajectories and lapse are similar away from the horizon, and the lapse is a bit different near the horizon, our slicing will be close to the background slicing, but slightly distorted toward the future near the horizon. In Sec. VI we try to quantify the significance of this distortion with a numerical study of the Kerr spacetime in these coordinates.

Other lapse possibilities can be considered which also produce a slicing similar to that of the Boyer-Lindquist background, algebraic slicings, for instance [20] $(1+\log)$, and a reparametrization of the maximal slicing by an $f(\alpha)$ such that the numerical lapse resembles the Boyer-Lindquist one even more closely. We performed such tests and checked that whenever the deviations from the Boyer-Lindquist lapse are close enough the results for the radiated waveforms and energies do not change notably, in agreement with the first order gauge invariance of ψ_4 and $\partial_t\psi_4$.

B. The spatial coordinates

The general idea here is to numerically compute physical quantities or geometrical invariants and relate them to their analytic expressions in the perturbatively preferred coordinate system. Curvature invariant methods have the distinct advantage that they can be applied to evolutions using numerically generated coordinates which are not understood analytically. On the other hand, the values of curvature invariants in the perturbed spacetime may be sensitive to perturbative distortions, making them less useful for identifying a background spacetime. In light of these effects, we pursue a combined approach, utilizing both gauge and geometrical information where each seems most appropriate. In the outer regions of our spatial slices we expect the gauge to be close to the quasi-isotropic gauge for Kerr data. Moving in from this to the interior region we expect, most importantly, two gauge effects. First, our slicing has the tendency (without a shift) to cause the coordinates to fall inward with evolution. We counteract this with a rescaling of the radius $r_{\rm Kerr} = r_{\rm Kerr}(r)$, making use of the $\mathcal{I}$ invariant which depends most significantly on the radial coordinate in the background slice, $\mathcal{I} = 3M^2/(r - ia\cos\theta)^6$. We use this relation and information about the numerical value of $\mathcal{I}$ to define the rescaled radius. To do this we need to produce one value of $\mathcal{I}$ for each constant r sphere in the numerical slice. The maximum value of $\int_0^{2\pi}\mathcal{I}d\varphi$ tends to lie on the equatorial symmetry plane of our binary black hole problem, where the $\mathcal{S}$ invariant also indicates relatively weaker distortions. This makes

$$\langle\mathcal{I}\rangle = \frac{1}{2\pi}\int_0^{2\pi}\mathcal{I}(r,\theta=\pi/2,\varphi)d\varphi, \tag{4.2}$$

$$r_{\rm Kerr} = \sqrt[6]{3M/\langle\mathcal{I}\rangle} \tag{4.3}$$

a practical definition that counteracts the coordinate infall.

Unlike on r, there are no obvious dynamical effects on the θ coordinate and it has been sufficient to adopt the numerical value $\cos\theta = z/\sqrt{(x^2+y^2+z^2)}$. We have successfully applied this remapping of coordinates already in the head-on collision case [5].

The second important coordinate effect, which becomes relevant when the total angular momentum is significant, is the result of frame dragging caused essentially by the difference between our vanishing shift and the nonvanishing Boyer-Lindquist shift. This effect drags the coordinates in the φ direction and has the effect of producing an off-diagonal distortion in the numerical metric. We can undo the frame dragging by attempting to restore the diagonal form of the Boyer-Lindquist three-metric.

We seek to set frame dragging gauge freedom by supplementing the Cartesian definition of φ with a correction that makes the metric component most strongly affected by frame dragging, $g_{r\phi}$, vanish:

$$\phi = \arctan[y/x] + \int (\hat{g}_{r\varphi}/\hat{g}_{\varphi\varphi})dr. \tag{4.4}$$

where the caret stands for the full numerically evolved metric. To see this, consider $\hat{g}_{ab}$ with no shift and transform to g_{ab} with ϕ shift by $\phi \to \hat{\varphi} - \varphi_{\rm Shift}(t,r,\theta)$. Thus

$$g_{r\phi} = 0 = \hat{g}_{r\varphi} - \partial_r \varphi_{\rm Shift} \hat{g}_{\varphi\varphi} \tag{4.5}$$

so that

$$\partial_r \varphi_{\rm Shift} = \frac{\hat{g}_{r\varphi}}{\hat{g}_{\varphi\varphi}}. \tag{4.6}$$

If g_{ab} is the Kerr metric

$$g_{t\varphi} = \hat{g}_{t\varphi} - \partial_t \varphi_{\rm Shift} \hat{g}_{\varphi\varphi} \tag{4.7}$$

so that

$$\partial_t \varphi_{\rm Shift} = -\frac{\hat{g}_{t\varphi}}{\hat{g}_{\varphi\varphi}} = -N^{\varphi}_{\rm Kerr} \tag{4.8}$$

is the Kerr shift, and

$$\partial_t^2 \varphi_{\rm Shift} = 0, \tag{4.9}$$

$$\varphi_{\rm Shift} = -tN^{\varphi}_{\rm Kerr}. \tag{4.10}$$

Equation (4.10) allows us to test how close our derived (from the block diagonal metric condition) shift correction is to the Boyer-Lindquist shift. The results of this comparison are displayed in Fig. 7. For two black holes evolving from the ISCO, the shift correction correctly reproduces the frame dragging effect outside the potential barrier of the system and evolution bring the shift closer to that of a single rotating Kerr hole.

We note that some means of fixing this frame-dragging degree of gauge freedom, as we have done here, is essential also if one wishes to speak meaningfully of the number of orbits the system has undergone in the strong field region during numerical simulations.

As already pointed out there is no unique way of choosing the coordinate transformations in order to bring them closer to that of the Kerr background. Our philosophy in this section has been to consider the simplest of these transformations that approaches the Boyer-Lindquist coordinates with enough accuracy for the binary–black-hole numerical simulations we are interested in. Obviously, other possibilities that would improve the accuracy of the procedure can be incorporated as needed. We also note that the optimal choice of coordinate transformation needed here may depend on the shift condition used in evolution and the coordinates used for the initial data. The use of a shift condition, such as minimal distortion (with the appropriate boundary conditions), which is naturally adapted to the stationarity Killing vector of the background Kerr spacetime [14], may, for example, eliminate frame dragging and thus reduce the need for a transformation such as (4.4).

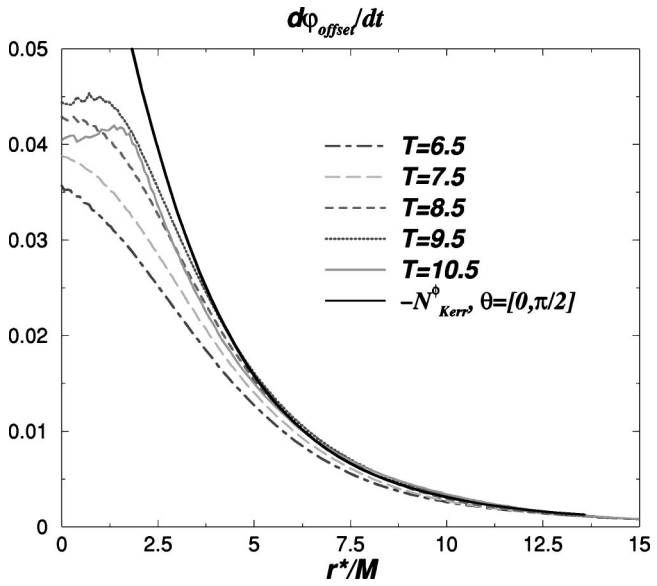

FIG. 7. The effective shift correction for black holes evolving from the ISCO compared to the analytic Kerr shift in Boyer-Lindquist coordinates for successive evolution times.

V. CONSTRUCTING THE CAUCHY DATA

Given the numerical metric g_{ij} and the extrinsic curvature K_{ij} derived as in Sec. II on a Cauchy hypersurface, and the coordinates of the background metric determined in Sec. IV, we proceed to compute the Weyl scalar ψ_4 and its background time derivative $\partial_t \psi_4$, the Cauchy data we will need to continue the evolution via the Teukolsky equation. As was discussed in Refs. [21–24], one can make a following 3 + 1 decomposition, using the basis $\theta^0 = dt$, $\theta^i = dx^i + N^i dt$, to get

$$\begin{aligned}\psi_4 = &-[R_{ijkl} + 2K_{i[k}K_{l]j}]n^i \bar{m}^j n^k \bar{m}^l + 8[K_{j[k,l]} \\ &+ \Gamma^p_{j[k}K_{l]p}]n^{[0}\bar{m}^{j]}n^k\bar{m}^l - 4[R_{jl} - K_{jp}K^p_l \\ &+ KK_{jl}]n^{[0}\bar{m}^{j]}n^{[0}\bar{m}^{l]},\end{aligned} \tag{5.1}$$

and its time derivative

$$\begin{aligned}\partial_t\psi_4 = &N^i\partial_i(\psi_4) - [\hat{\partial}_0 R_{ijkl}]n^i\bar{m}^j n^k\bar{m}^l + 8[\hat{\partial}_0 K_{j[k,l]} \\ &+ \hat{\partial}_0\Gamma^p_{j[k}K_{l]p} + \Gamma^p_{j[k}\hat{\partial}_0 K_{l]p}]n^{[0}\bar{m}^{j]}n^k\bar{m}^l - 4[\hat{\partial}_0 R_{jl} \\ &- 2K^p_{(l}\hat{\partial}_0 K_{j)p} - 2NK_{jp}K^p_q K^q_l + K_{jl}\hat{\partial}_0 K \\ &+ K\hat{\partial}_0 K_{jl}]n^{[0}\bar{m}^{j]}n^{[0}\bar{m}^{l]} - 2\{\psi_4(l_i\hat{\Delta} - m_i\bar{\delta})N^i \\ &+ \psi_3(n_i\bar{\delta} - \bar{m}_i\hat{\Delta})N^i\},\end{aligned} \tag{5.2}$$

where the last term extends the expression in Ref. [23], having been added to take into account the variation of the tetrad terms $\hat{\partial}_0[\mathbf{n\bar{m}n\bar{m}}]$. Here $\hat{\Delta}=n^\mu\partial_\mu$, $\bar{\delta}=\bar{m}^\mu\partial_\mu$, and

$$\psi_3=-[R_{ijkl}+2K_{i[k}K_{l]j}]l^i n^j \bar{m}^k n^l+4[K_{j[k,l]}+\Gamma^p_{j[k}K_{l]p}] \times(l^{[0}n^{j]}\bar{m}^k n^l-n^{[0}\bar{m}^{j]}l^k n^{l)})-2[R_{jl}-K_{jp}K^p_l+KK_{jl}] \times(l^{[0}n^{j]}\bar{m}^0 n^{l)}-l^{[0}n^{j]}n^0\bar{m}^{l)}), \tag{5.3}$$

where the background (null and complex) tetrad $(l^\mu,n^\mu,m^\mu,\bar{m}^\mu)$ is specified in the subsection below.

The derivatives involved in the above expressions can be computed in terms of the initial data on the Cauchy hypersurface as in Eq. (A19) in the Appendix.

With the tetrad specified, the foregoing formulas are coordinate independent. Therefore the only adjustment needed to specify initial data for the evolution equations is to insert the appropriate background quantities in the above equations. In particular, taking N and $N_{(i)}$ respectively as the zeroth order Kerr lapse and shift, $N^{(0)}=\sqrt{\Delta\Sigma/\Omega}$ and $N^{(0)}_{(i)}=[0,0,-2aMr/\Omega]$, allows us to compute $\partial_t\psi_4$ directly with respect to the background Boyer-Lindquist time, thus avoiding additional perturbations introduced if one computes the numerical derivative by finite differences of ψ_4 on two successive slices.

A. The tetrad

A null and complex ''exact'' tetrad (i.e. orthonormal in the numerical spacetime) must be chosen such that it reduces in the linear regime to the choice made in our perturbation treatment of the final Kerr hole, the Kinnersley tetrad [9]. In Boyer-Lindquist coordinates the background tetrad vectors are

$$l^\mu_{\rm Kin}=\frac{1}{\Delta}[(r^2+a^2),\Delta,0,a], \tag{5.4a}$$

$$n^\mu_{\rm Kin}=\frac{1}{2\Sigma}[(r^2+a^2),-\Delta,0,a], \tag{5.4b}$$

$$m^\mu_{\rm Kin}=\frac{1}{\sqrt{2}(r+ia\cos\theta)}\left[\frac{ia}{\sin\theta},0,1,\frac{i}{\sin\theta}\right]. \tag{5.4c}$$

The Kinnersley tetrad is particularly well suited for perturbation studies because it has the property that l^μ and n^μ are chosen to lie along the (background) principal null directions (PND's) of the Weyl tensor in such a way that one can derive decoupled perturbation equations. In terms of the $3+1$ basis of Eqs. (5.1)–(5.3), we have

$$l^\mu=[N^{(0)}l^0_{\rm Kin},l^i+N^{i(0)}l^0_{\rm Kin}], \tag{5.5a}$$

$$n^\mu=[N^{(0)}n^0_{\rm Kin},n^i+N^{i(0)}n^0_{\rm Kin}], \tag{5.5b}$$

$$m^\mu=[N^{(0)}m^0_{\rm Kin},l^i+N^{i(0)}m^0_{\rm Kin}]. \tag{5.5c}$$

To numerically determine an exact tetrad we could in principle search for possible candidates for two of the PND's of the Weyl tensor. One could, of course, try to pick up some null directions in our numerical spacetime $g^{num}_{\mu\nu}$ which we know are close to the PND's in Kerr spacetime whenever $g^{num}_{\mu\nu}$ is a perturbation of the Kerr spacetime. However, this turns out to be a bad choice because the PND's do not behave analytically under analytic perturbations of Kerr spacetime. The reason is that the principal null directions of Kerr spacetime are double principal null directions of the Weyl tensor, which in general will split under the perturbation. It turns out that the splitting of eigenvectors of an endomorphism under a perturbation of order ϵ behaves in general as some fractional power of ϵ (hence nonsmoothly). So the principal null directions will be too strongly perturbed.

An alternative and more effective procedure to define an exact tetrad that has the required property in the linear regime is the following. (a) We assume the following $3+1$ decomposition of the tetrad:

$$\tilde{l}^\mu=\frac{1}{\sqrt{2}}(u^\mu+r^\mu), \tag{5.6a}$$

$$\tilde{n}^\mu=\frac{1}{\sqrt{2}}(u^\mu-r^\mu), \tag{5.6b}$$

$$\tilde{m}^\mu=\frac{1}{\sqrt{2}}(\theta^\mu+i\varphi^\mu), \tag{5.6c}$$

where u^μ is the normalized timelike unit normal to the hypersurface and $r^\mu=[1,v^a_2]$, $\theta^\mu=[0,v^a_3]$, $\varphi^\mu=[0,v^a_1]$ are orthonormal vectors pointing along the numerically defined coordinate directions. (b) We thus identify the set of null rotations to bring Eq. (5.6) to the form (5.5), in order to make it consistent with the tetrad assumed in the perturbative calculation.

Step a is straightforward. Begin with real vectors aligned with the numerical space φ and radial directions, which in Cartesian coordinates read

$$v^a_1=[-y,x,0],$$

$$v^a_2=[x,y,z],$$

$$v^a_3=\det(g)^{1/2}g^{ad}\epsilon_{dbc}v^b_1v^c_2. \tag{5.7}$$

We then redefine these, to achieve orthonormalization. It is important to begin the ortho-normalization procedure with the azimuthal direction vector v^a_1 which is not affected by the frame-dragging effect discussed in Sec. II B. At each step, a Gram-Schmidt procedure is then used to ensure that the triad remains orthonormal, so that

$$v^a_1\rightarrow\frac{v^a_1}{\sqrt{\omega_{11}}},$$

$$v_2^a \to \frac{(v_2^a - v_1^a \omega_{12})}{\sqrt{\omega_{22}}},$$

$$v_3^a \to \frac{(v_3^a - v_1^a \omega_{13} - v_2^a \omega_{23})}{\sqrt{\omega_{33}}},$$

where $\omega_{ij} = (v_i^a v_j^b g_{ab})$. In the case of Kerr spacetime one finds, in Boyer-Lindquist coordinates,

$$u^\mu = \left[\sqrt{\frac{\Delta\Sigma}{\Omega}}, 0, 0 \right], \tag{5.8a}$$

$$r^\mu = [1, v_2^a] = \left[1, \sqrt{\frac{\Delta}{\Sigma}}, 0, 0 \right], \tag{5.8b}$$

$$\theta^\mu = [0, v_3^a] = \left[0, 0, \frac{1}{\sqrt{\Delta}}, 0 \right], \tag{5.8c}$$

$$\varphi^\mu = [0, v_1^a] = \left[0, 0, 0, \frac{1}{\sin\theta} \sqrt{\frac{\Sigma}{\Omega}} \right], \tag{5.8d}$$

normalized such that $-u_\mu u^\mu = r_\mu r^\mu = \theta_\mu \theta^\mu = \varphi_\mu \varphi^\mu = 1$ so that the inverse metric can be expressed as $g^{\mu\nu} = 2(m^{(\mu} \overline{m}^{\nu)} - l^{(\mu} \overline{n}^{\nu)})$.

For step b identify a combination of null rotations of types I and II parametrized by A, and a type III (boost) null rotation parametrized by F_A and F_B which bring the orthonormal tetrad (5.6) to the form (5.5) for the unperturbed case. The transformation

$$l^\mu = \frac{F_A}{2} \{ [\sqrt{(A^2+1)+1}] \tilde{l}^\mu + [\sqrt{(A^2+1)-1}] \tilde{n}^\mu - iA(\tilde{m}^\mu - \overline{\tilde{m}}^\mu) \}, \tag{5.9a}$$

$$n^\mu = \frac{F_A^{-1}}{2} \{ [\sqrt{(A^2-1)+1}] \tilde{l}^\mu + [\sqrt{(A^2+1)+1}] \tilde{n}^\mu - iA(\tilde{m}^\mu - \overline{\tilde{m}}^\mu) \}, \tag{5.9b}$$

$$m^\mu = \frac{F_B}{2} \{ [\sqrt{(A^2+1)+1}] \tilde{m}^\mu - [\sqrt{(A^2+1)-1}] \overline{\tilde{m}}^\mu + iA(\tilde{l}^\mu + \tilde{n}^\mu) \} \tag{5.9c}$$

achieves this with $A = a \sin\theta \sqrt{\Delta/\Omega}$, $F_A = \sqrt{2\Sigma/\Delta}$ and $F_B = \sqrt{\Sigma}/(r + ia\cos\theta)$, thereby producing a tetrad consistent with the tetrad assumed in the perturbative calculation.

In practice we perform the tetrad transformation indirectly, implementing its effect on the set of Weyl scalars $(\psi_0, \ldots, \psi_4)$ as described in the Appendix, Eq. (A24).

VI. THE TEUKOLSKY EQUATION

Perturbations of a rotating Kerr black hole are described by the well known Teukolsky equation [9], which is derived from the Newman-Penrose formalism. The Weyl scalar ψ_4 that represents outgoing gravitational radiation satisfies a decoupled wave equation

$$\{(\Delta + 4\mu + \overline{\mu} + 3\gamma - \overline{\gamma})(D + 4\epsilon - \rho) - (\overline{\delta} + 3\alpha + \overline{\beta} + 4\pi - \overline{\tau}) \times (\delta + 4\beta - \tau) - 3\psi_2^{(0)}\} \psi_4^{(1)} = 0. \tag{6.1}$$

In this generic form the Teukolsky equation is manifestly independent of the choice of coordinate system used to describe the Kerr background and its perturbations. In the foregoing equation the usual notation for spin coefficients $\alpha, \beta, \ldots$ was used and $\hat{\Delta} = n^\mu \partial_\mu$, $\delta = m^\mu \partial_\mu$, and $D = l^\mu \partial_\mu$ represent directional derivatives.

For the applications in this paper we consider Boyer-Lindquist coordinates (t, r, θ, ϕ) and the Kinnersley tetrad. The Teukolsky equation then reads

$$\left[\frac{(r^2+a^2)^2}{\Delta} - a^2 \sin^2\theta \right] \frac{\partial^2\psi}{\partial t^2} + \frac{4Mar}{\Delta} \frac{\partial^2\psi}{\partial t \partial \phi} + \left[\frac{a^2}{\Delta} - \frac{1}{\sin^2\theta} \right] \frac{\partial^2\psi}{\partial \phi^2} - \Delta^2 \frac{\partial}{\partial r} \left(\frac{1}{\Delta} \frac{\partial\psi}{\partial r} \right) - \frac{1}{\sin\theta} \frac{\partial}{\partial\theta} \left(\sin\theta \frac{\partial\psi}{\partial\theta} \right) + 4 \left[\frac{M(r^2-a^2)}{\Delta} - r - ia\cos\theta \right] \frac{\partial\psi}{\partial t} + 4 \left[\frac{a(r-M)}{\Delta} + \frac{i\cos\theta}{\sin\theta} \right] \frac{\partial\psi}{\partial\phi} + (4\cot^2\theta + 2)\psi = 0, \tag{6.2}$$

where $\psi = [r - ia\cos(\theta)]^4 \psi_4$.

This formulation has several advantages: (i) It is a first order gauge invariant description. (ii) It does not rely on any frequency or multipole decomposition. (iii) It can be used to evolve $3+1$ dimensional spacetimes without any assumption about symmetries (to deal with the final stage of orbiting binary black holes). (iv) The Weyl scalars are objects defined in the full nonlinear theory and it can be argued that evolving them with the linear theory provides a reliable description of the perturbations [25]. In addition, the Newman-Penrose formulation constitutes a simple and elegant framework to organize higher order perturbations [24].

The numerical integration of the linear Teukolsky equation in the time domain using Boyer-Lindquist coordinates is done closely following Ref. [26]. We use the Lax-Wendroff algorithm, using the standard tortoise coordinate r^*,

$$r^* = r + \frac{r_+^2 + a^2}{r_+ - r_-} \ln\left| \frac{r - r_+}{2M} \right| - \frac{r_-^2 + a^2}{r_+ - r_-} \ln\left| \frac{r - r_-}{2M} \right|,$$

$$r_\pm = M \pm \sqrt{M^2 - a^2}, \tag{6.3}$$

which naturally leads to excision of the black hole interior and constant characteristic wave speed. We impose static boundary conditions on the internal boundary (event horizon of the Kerr background) and radiative boundary conditions

on the exterior boundary. Frame dragging effects are taken care of by the background Boyer-Lindquist shift. Thus, this formulation has all the ingredients to allow for an indefinite stable evolution. In practice it provides an accurate evolution for the few hundreds of M of relevant signal generated in the final stages of black hole merger. Since the Kerr background has the axial killing vector ∂_ϕ we can Fourier decompose ψ_4 into $e^{im\phi_{KS}}$ modes. In particular, for numerical convenience, we use the Kerr-Schild ϕ_{KS},

$$\phi_{KS}=\phi+\frac{a}{r_+-r_-}\ln\left|\frac{r}{r_+}-1\right|-\frac{a}{r_+-r_-}\ln\left|\frac{r}{r_-}-1\right|. \tag{6.4}$$

This allows us to reduce the dimensionality of the Teukolsky equation from $3+1$ to $2+1$. In addition this decomposition into modes can be applied to the output of the full numerical code with the advantage of handling 2D instead of 3D fields. Typical evolutions of the Teukolsky equation used a grid size of $n_\theta \times n_{r*}=40\times 1200$, with $-18<r*/M<78$ for signals of $t\sim 100M$, and we filled in initially with zeros (or used extrapolations) the grid points outside the full numerical domain. Finally, the computation of the energy and momenta radiated is performed using the formulas of Ref. [24], Sec. III C.

It is worth stressing here that the Teukolsky equation can be written in any coordinate system. We are using it in the Boyer-Lindquist coordinates for present convenience, but if full numerical codes including excision black hole interiors turn out to be more practical in Kerr-Schild-like coordinates, it may be convenient to evolve perturbations in Kerr-Schild slices of the Kerr metric [27].

VII. APPLICATION TO A SINGLE ROTATING KERR HOLE

We have done extensive testing of our method on various toy models. In an earlier incarnation, we tried our approach successfully on axisymmetric head-on collision. As we have described, we have done a lot of work generalizing our method to include orbital cases with angular momentum on the final black hole. We have checked our equations explicitly on exact Boyer-Lindquist Kerr data, but in our real numerical simulations we will not reproduce the Boyer-Lindquist coordinates exactly and it is useful to get some measure of how important the coordinate differences are for the radiation. Additionally, our calculation requires the use of four computer codes, a code for the numerical simulation (CACTUS [28]), a specialized code (called ZORRO) running within the simulation that calculates all the quantities needed for producing Cauchy data (see the Appendix), a code (called TEUKCAUCHY) that runs after the simulation defining the background black hole and constructing the Cauchy data from the output of the evolution on various time slices, and the Teukolsky evolution code (TEUKCODE). The Kerr case has been a key source of rigorous tests of all these codes.

We performed a highly nontrivial test of our setup by applying the entire procedure to Kerr initial data, evolving a single Kerr hole fully numerically, finding a ''background'' black hole in the numerical data and defining a tetrad, extracting the Cauchy data and continuing its evolution with the Teukolsky equation. Ideally, the final result should produce no radiation. In practice, the computed radiation energy and waveforms will give us a measure of the error with which we can determine such quantities.

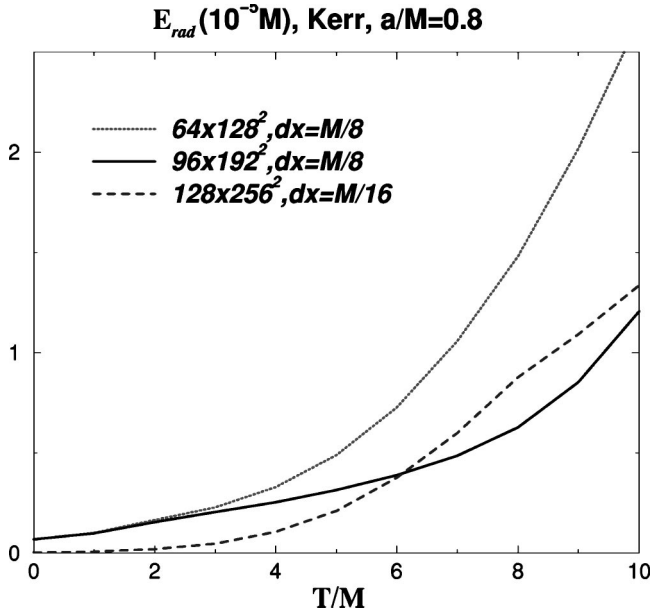

FIG. 8. The total radiated energy for an evolved Kerr hole for different resolutions and boundary locations.

This is a nontrivial test because the full numerical evolution is performed with vanishing shift and the singularity avoiding maximal slicing. This is in contrast to the Boyer-Lindquist lapse and the nonvanishing Boyer-Lindquist shift for rotation parameter $a/M=0.8$ in the example shown in Fig. 8. In addition the Cauchy data for ψ_4 and $\partial_t\psi_4$ are computed with a tetrad adapted to the numerical spacetime, which must then be transformed according to Sec. V A in order to nearly reproduce the Kinnersley tetrad in the perturbative limit. These complications mean, in particular, that the data passed between our first three codes are not expected to be approximately vanishing, but must sum to zero in the end. In practice our result is subject to both numerical error and false radiation caused by an inexact identification of the background coordinates and tetrad, perhaps producing nontrivial Cauchy data which we then evolve via the Teukolsky equation. The results of the whole procedure are summarized in Fig. 8. The levels of spurious radiation are around $10^{-5}M$. Results after relatively short evolution times converge quadratically toward zero with increasing resolution. The longer evolutions are affected by the location of a close exterior boundary, and are improved when we move the boundary outward by 50%. (As discussed above we will use much more distant outer boundaries for our astrophysical applications.) All this indicates that the coordinate effects are, so far, smaller than the numerical effects, which in turn tend to produce radiation about two orders of magnitude smaller than the radiation we are interested in. Notably these results are achieved with lower resolutions and closer boundaries than the typical resolutions of runs we performed for two

black holes starting from the ISCO configuration used in Ref. [6].

For the sake of completeness we mention two further tests that we performed for two black hole initial data: (i) The mass scaling of the whole procedure. Since Einstein equations scale with the total ADM mass, we made a full numerical run with initial mass equal to 2 and compared the scaling of the Cauchy data, post-processing and final waveforms with the mass 1 case. This proved to be a very useful test for the corresponding set of four codes we used to compute each of the above stages. (ii) The initial separation of the holes. When we reduce this from that of the ISCO to one quarter of that value we reach the close limit regime and can compare with the results from the known analytic expressions [29] and scaling for the separation as well as for the angular dependence of ψ_4 and $\partial_t \psi_4$.

VIII. DISCUSSION

The Lazarus approach to binary black holes combines three treatments, each adapted to one of three stages of the dynamics: the far-limit, nonlinear-interaction, and close-limit (one black hole) regimes. In this paper we have provided a detailed explanation of how numerical simulation and Teukolsky equation perturbative dynamics can be interfaced to provide a complete description of gravitational radiation arising from the post-orbital binary–black-hole dynamics.

This technology makes it possible, for the first time, to apply numerical relativity to the nonlinear dynamical interaction of these systems. In our approach to this unknown regime, we have identified several parameter sequences that make a connection to better-studied cases: an L sequence that allows us to increase the separation from the close-limit regime to the ISCO, an α sequence that allows us to connect boosted head-on collisions studied in 2D to the ISCO with a fixed magnitude of each black hole's momentum, and a P sequence through which we connect to head-on collisions of resting black holes by varying the magnitude of the momentum to the ISCO value [6]. These important studies will give us some understanding of how the dynamics from ISCO configurations relate to and differ from the simpler problems treated so far by numerical simulations and close-limit studies.

After establishing such a basis for understanding the near ISCO regime dynamics we can reach out further, and seek to firmly establish the relation of these ISCO black hole configurations to astrophysics. As we have discussed in detail for the numerical simulation/close-limit interface, the dual approach to dynamics in overlapping validity regions provides a vital consistency check on the reliability of the results. A key goal, which we can now begin to approach, is to provide the same sort of consistency studies for the far-limit/numerical simulation interface and to thereby establish a firm astrophysical foundation for expensive, and difficult, numerical work. Again, a handful of initial data sequences are appropriate for beginning to evaluate the connection of numerical/close-limit results to astrophysical problems. Within the effective-potential method which we have taken advantage of in order to define ISCO data there is a natural PI sequence of pre-ISCO stable circular orbits. Moving up within this sequence towards more separated black holes asymptotically eliminates the features of these data which may be less astrophysical. Similarly, it is possible to define curves through the parameter space of our initial data family which approach the trajectories defined by the Buonanno-Damour extension of the post-Newtonian method. The application of more advanced numerical techniques [30], which we are presently undertaking, should make it possible to begin generating waveforms from farther up these sequences. Still, though, the effective potential method initial data sequence is an imperfect substiute for robust interface with the post-Newtonian method, which we expect to be ultimately required. Since a primary concern about the astrophysical relevance of numerical/close-limit results is artificial radiation content in the initial data, another useful line of research is comparison studies of waveform alternative initial data sets which would be equivalent in their astrophysical interpretation. These will provide a measure of the significance of this interpretive indeterminacy to the gravitational radiation. Promising work with evolutions from Kerr-Schild-like initial data, for which an alternative application of the Lazarus approach is under development [31], should provide an example of such comparative work.

Another area of study that can now be pursued is to develop some preliminary indications of the effect spin has on the waveforms generated in the post-inspiral dynamics. The effective potential approach provides a description [32] of the effect small amounts of individual black hole spin have on the ISCO initial data. We are applying our approach in the first instance to cases of spin parallel and antiparallel to the orbital angular momentum.

Eventually numerical simulations will run routinely for hundreds or thousands of M, having begun from established astrophysical data. But the possibility of observation is beginning almost immediately, and until now we have not met the needs of observers who consider that any additional information about the the final stage of binary black holes may be extremely important [33]. Our efforts have shown that a crucial requirement for producing results relevant to observers is to adapt numerical evolutions to astrophysical problems. Numerical relativity is ready, now, to begin answering questions about binary black holes in the near ISCO and pre-ISCO regime.

ACKNOWLEDGMENTS

We wish to thank especially B. Brügmann and R. Takahashi for many contributions to this work. We also acknowledge many helpful discussions with P. Laguna, R. Price, and B. Schutz. M.C. was also supported by the IHRP program of the European Union (through Grant No. HPMF-CT-1999-00334). All our numerical computations were performed at AEI and NCSA Origin 2000s.

APPENDIX: A PRACTICAL CONSTRUCTION OF THE CAUCHY DATA

Here we describe a procedure for calculating ψ_4 that allows us to cleanly separate the specification of the back-

ground black hole from the numerical simulation, as is practical for studying variations of the background metric and background coordinates. Since we have not yet determined the background black hole at the time of evolution we must compute a larger set of quantities which can then be transformed to the desired result after the background is specified. The steps are as follows.

(a) Compute the numerical $3+1$ tetrad components as in Eq. (5.6).

(b) With this tetrad, using the Cauchy data on a numerical time slice directly compute all five Weyl scalars $\psi_0, \ldots, \psi_4$ and their time variations $\hat{\partial}_0\psi_0, \ldots, \hat{\partial}_0\psi_4$ as follows:

$$\psi_4 = R_{ijkl} n^i \overline{m}^j n^k \overline{m}^l + 2R_{0jkl}(n^0 \overline{m}^j n^k \overline{m}^l - \overline{m}^0 n^j n^k \overline{m}^l) + R_{0j0l}(n^0 \overline{m}^j n^0 \overline{m}^l + \overline{m}^0 n^j \overline{m}^0 n^l - 2n^0 \overline{m}^j \overline{m}^0 n^l), \tag{A1}$$

$$\psi_3 = R_{ijkl} l^i n^j \overline{m}^k n^l + R_{0jkl}(l^0 n^j \overline{m}^k n^l - n^0 \overline{m}^j l^k n^l - n^0 l^j \overline{m}^k n^l + \overline{m}^0 n^j l^k n^l) + R_{0j0l}(l^0 n^j \overline{m}^0 n^l - l^0 n^j n^0 \overline{m}^l - n^0 l^j \overline{m}^0 n^l + n^0 l^j n^0 \overline{m}^l), \tag{A2}$$

$$\psi_2 = R_{ijkl} l^i m^j \overline{m}^k n^l + R_{0jkl}(l^0 m^j \overline{m}^k n^l - n^0 \overline{m}^j l^k m^l - m^0 l^j \overline{m}^k n^l + \overline{m}^0 n^j l^k m^l) + R_{0j0l}(l^0 m^j \overline{m}^0 n^l - l^0 m^j n^0 \overline{m}^l - m^0 l^j \overline{m}^0 \overline{m}^l + n^0 l^j m^0 \overline{m}^l), \tag{A3}$$

$$\psi_1 = R_{ijkl} n^i l^j m^k l^l + R_{0jkl}(n^0 l^j m^k l^l - l^0 m^j n^k l^l - l^0 n^j m^k l^l + m^0 l^j n^k l^l) + R_{0j0l}(n^0 l^j m^0 l^l - n^0 l^j l^0 m^l - l^0 n^j m^0 l^l + l^0 n^j l^0 m^l) \tag{A4}$$

$$\psi_0 = R_{ijkl} l^i m^j l^k m^l + 2R_{0jkl}(l^0 m^j l^k m^l - m^0 l^j l^k m^l) + R_{0j0l}(l^0 m^j l^0 m^l + m^0 l^j m^0 l^l - 2l^0 m^j m^0 l^l), \tag{A5}$$

where

$$R_{ijkl} = R_{ijkl} + 2K_{i[k}K_{l]j},$$
$$R_{0jkl} = -4[K_{j[k,l]} + \Gamma^p_{j[k}K_{l]p}],$$
$$R_{0j0l} = R_{jl} - K_{jp}K^p_l + KK_{jl}. \tag{A6}$$

We compute the time variations only from data on the slice:

$$\hat{\partial}_0\psi_4 = \hat{\partial}_0 R_{ijkl} n^i \overline{m}^j n^k \overline{m}^l + 2\hat{\partial}_0 R_{0jkl}(n^0 \overline{m}^j n^k \overline{m}^l - \overline{m}^0 n^j n^k \overline{m}^l) + \hat{\partial}_0 R_{0j0l}(n^0 \overline{m}^j n^0 \overline{m}^l + \overline{m}^0 n^j \overline{m}^0 n^l - 2n^0 \overline{m}^j \overline{m}^0 n^l), \tag{A7}$$

$$\hat{\partial}_0\psi_3 = \hat{\partial}_0 R_{ijkl} l^i n^j \overline{m}^k n^l + \hat{\partial}_0 R_{0jkl}(l^0 n^j \overline{m}^k n^l - n^0 \overline{m}^j l^k n^l - n^0 l^j \overline{m}^k n^l + \overline{m}^0 n^j l^k n^l) + \hat{\partial}_0 R_{0j0l}(l^0 n^j \overline{m}^0 n^l - l^0 n^j n^0 \overline{m}^l - n^0 l^j \overline{m}^0 n^l + n^0 l^j n^0 \overline{m}^l), \tag{A8}$$

$$\hat{\partial}_0\psi_2 = \hat{\partial}_0 R_{ijkl} l^i m^j \overline{m}^k n^l + \hat{\partial}_0 R_{0jkl}(l^0 m^j \overline{m}^k n^l - n^0 \overline{m}^j l^k m^l - m^0 l^j \overline{m}^k n^l + \overline{m}^0 n^j l^k m^l) + \hat{\partial}_0 R_{0j0l}(l^0 m^j \overline{m}^0 n^l - l^0 m^j n^0 \overline{m}^l - m^0 l^j \overline{m}^0 \overline{m}^l + n^0 l^j m^0 \overline{m}^l), \tag{A9}$$

$$\hat{\partial}_0\psi_1 = \hat{\partial}_0 R_{ijkl} n^i l^j m^k l^l + \hat{\partial}_0 R_{0jkl}(n^0 l^j m^k l^l - l^0 m^j n^k l^l - l^0 n^j m^k l^l + m^0 l^j n^k l^l) + \hat{\partial}_0 R_{0j0l}(n^0 l^j m^0 l^l - n^0 l^j l^0 m^l - l^0 n^j m^0 l^l + l^0 n^j l^0 m^l), \tag{A10}$$

$$\hat{\partial}_0\psi_0 = \hat{\partial}_0 R_{ijkl} l^i m^j l^k m^l + 2\hat{\partial}_0 R_{0jkl}(l^0 m^j l^k m^l - m^0 l^j l^k m^l) + \hat{\partial}_0 R_{0j0l}(l^0 m^j l^0 m^l + m^0 l^j m^0 l^l - 2l^0 m^j m^0 l^l). \tag{A11}$$

The derivatives involved in the above expressions can be computed in terms of the data on the Cauchy hypersurface using Einstein's equations:

$$\hat{\partial}_0 R_{ijkl} = -4N_{(0)}\left\{K_{i[k}R_{l]j} - K_{j[k}R_{l]i} - \frac{1}{2}R(K_{i[k}g_{l]j} - K_{j[k}g_{l]i})\right\} + 2g_{i[k}\hat{\partial}_0 R_{l]j} - 2g_{j[k}\hat{\partial}_0 R_{l]i} - g_{i[k}g_{l]j}\partial_0 R + 2K_{i[k}\partial_0 K_{l]j} - 2K_{j[k}\partial_0 K_{l]i}, \tag{A12}$$

$$\hat{\partial}_0 R_{0jkl} = \partial_0 K_{j[k,l]} + \hat{\partial}_0\Gamma^p_{j[k}K_{l]p} + \Gamma^p_{j[k}\hat{\partial}_0 K_{l]p}, \tag{A13}$$

$$\hat{\partial}_0 R_{0j0l} = [\partial_0 R_{jl} - 2K^p_{(l}\partial_0 K_{j)p} - 2NK_{jp}K^p_q K^q_l + K_{jl}\partial_0 K + K\partial_0 K_{jl}], \tag{A14}$$

where

$$\hat{\partial}_0 K = NK_{pq}K^{pq} - \nabla^2 N, \tag{A15}$$

$$\hat{\partial}_0 K_{ij} = N[\overline{R}_{ij} + KK_{ij} - 2K_{ip}K^p{}_j - N^{-1}\overline{\nabla_i\nabla_j}N], \tag{A16}$$

$$\hat{\partial}_0 R = 2K^{pq}\partial_0 K_{pq} + 4NK_{pq}K^p_s K^{sq} - 2K\partial_0 K, \tag{A17}$$

$$\hat{\partial}_0 \overline{R}_{ij} = \overline{\nabla}_k(\hat{\partial}_0\overline{\Gamma}^k_{ij}) - \overline{\nabla}_j(\hat{\partial}_0\overline{\Gamma}^k_{ik}), \tag{A18}$$

$$\hat{\partial}_0\overline{\Gamma}^k_{ij} = -2\overline{\nabla}_{(i}(NK_{j)}{}^k) + \overline{\nabla}^k(NK_{ij}). \tag{A19}$$

These time variations may be precisely the background time derivatives we want if have already specified the background spacetime and can set $N=N_{(0)}$ as the background lapse. On the other hand when we want to determine the background independently of the numerical simulation code we can produce the required information for later processing from all five quantities with the choice $N=1$.

(c) Next define the background coordinate system as described in Sec. IV. This allows us now to refer to quantities defined in the background coordinates. If we have used N

$=1$ in constructing the time variations we must next translate the time variations calculated above to genuine background time derivatives with a set of corrections for the effect of the background lapse and shift. For the lapse,

$$\hat{\partial}_0\psi_0 \to \alpha\hat{\partial}_0\psi_0 + 2\,\alpha_{,\hat{r}}\psi_0 + 2\,\alpha_{,\hat{\theta}}\psi_1, \tag{A20a}$$

$$\hat{\partial}_0\psi_1 \to \alpha\hat{\partial}_0\psi_1 + \alpha_{,\hat{r}}\psi_1 + \frac{1}{2}\alpha_{,\hat{\theta}}(\psi_0 + 3\psi_2), \tag{A20b}$$

$$\hat{\partial}_0\psi_2 \to \alpha\hat{\partial}_0\psi_2 + \alpha_{,\hat{\theta}}(\psi_1 + \psi_3), \tag{A20c}$$

$$\hat{\partial}_0\psi_3 \to \alpha\hat{\partial}_0\psi_3 - \alpha_{,\hat{r}}\psi_3 + \frac{1}{2}\alpha_{,\hat{\theta}}(\psi_4 + 3\psi_2), \tag{A20d}$$

$$\hat{\partial}_0\psi_4 \to \alpha\hat{\partial}_0\psi_4 - 2\,\alpha_{,\hat{r}}\psi_4 + 2\,\alpha_{,\hat{\theta}}\psi_3, \tag{A20e}$$

where $\alpha_{,\hat{r}}$ and $\alpha_{,\hat{\theta}}$ are related to the lapse for the background Kerr metric,

$$\alpha_{,\hat{r}} = \frac{1}{\sqrt{g_{rr}}}N_{,r} = \sqrt{\frac{\Delta}{\Sigma}}N_{,r}$$
$$\alpha_{,\hat{\theta}} = \frac{1}{\sqrt{g_{\theta\theta}}}N_{,\theta} = \sqrt{\frac{1}{\Sigma}}N_{,\theta}. \tag{A21}$$

The shift corrections are

$$\hat{\partial}_0\psi_0 \to \hat{\partial}_0\psi_0 + i\,\beta^{\hat{\varphi}}_{,\hat{\theta}}\psi_0 + i\,\beta^{\hat{\varphi}}_{,\hat{r}}\psi_1 + N^k\partial_k\psi_0, \tag{A22a}$$

$$\hat{\partial}_0\psi_1 \to \hat{\partial}_0\psi_1 + \frac{i}{2}\beta^{\hat{\varphi}}_{,\hat{r}}(\psi_0 + \psi_2) - \frac{i}{2}\beta^{\hat{\varphi}}_{,\hat{\theta}}(\psi_1 - \overline{\psi}_1) + \frac{i}{2}\beta^{\hat{\varphi}}_{,\hat{r}}(\psi_2 - \overline{\psi}_2) + N^k\partial_k\psi_1, \tag{A22b}$$

$$\hat{\partial}_0\psi_2 \to \hat{\partial}_0\psi_2 + \frac{i}{2}\beta^{\hat{\varphi}}_{,\hat{r}}(\psi_1 + \psi_3) + N^k\partial_k\psi_2, \tag{A22c}$$

$$\hat{\partial}_0\psi_3 \to \hat{\partial}_0\psi_3 + \frac{i}{2}\beta^{\hat{\varphi}}_{,\hat{r}}(\psi_4 + \psi_2) + \frac{i}{2}\beta^{\hat{\varphi}}_{,\hat{\theta}}(\psi_3 - \overline{\psi}_3) + \frac{i}{2}\beta^{\hat{\varphi}}_{,\hat{r}}(\psi_2 - \overline{\psi}_2) + N^k\partial_k\psi_3, \tag{A22d}$$

$$\hat{\partial}_0\psi_4 \to \hat{\partial}_0\psi_4 - i\,\beta^{\hat{\varphi}}_{,\hat{\theta}}\psi_4 + i\,\beta^{\hat{\varphi}}_{,\hat{\theta}}\psi_3 + N^k\partial_k\psi_4, \tag{A22e}$$

where $\beta^{\hat{\varphi}}_{,\hat{r}}$ and $\beta^{\hat{\varphi}}_{,\hat{\theta}}$ are related to the lapse for the background Kerr metric,

$$\beta^{\hat{\varphi}}_{,\hat{r}} = \sqrt{\frac{g_{\varphi\varphi}}{g_{rr}}}\beta^{\varphi}{}_{,r} = \sqrt{\Delta\Omega}\,\frac{\sin\theta}{\Sigma}\beta^{\varphi}{}_{,r},$$
$$\beta^{\hat{\varphi}}_{,\hat{\theta}} = \sqrt{\frac{g_{\varphi\varphi}}{g_{\theta\theta}}}\beta^{\varphi}{}_{,\theta} = \sqrt{\Omega}\,\frac{\sin\theta}{\Sigma}\beta^{\varphi}{}_{,\theta}. \tag{A23}$$

(d) The Weyl scalars corresponding to the transformed tetrad defined in Eq. (5.9), $\tilde{\Psi}_4$ and $\partial_t\tilde{\Psi}_4$, can then be respectively expressed as a linear combination of the five numerical-tetrad Weyl scalars $\psi_4, \ldots, \psi_0$ and the $\hat{\partial}_0\psi_4 \ldots \hat{\partial}_0\psi_0$, as given in Eqs. (A22), with coefficients depending on the background coordinates r and θ, and on M and a:

$$\tilde{\psi}_4 = \frac{1}{4F_A^2F_B^2}[(\sqrt{A^2+1}-1)^2\psi_0 + 4iA(\sqrt{A^2+1}-1)\psi_1 - 6A^2\psi_2 - 4iA(\sqrt{A^2+1}+1)\psi_3 + (\sqrt{A^2+1}+1)^2\psi_4], \tag{A24}$$

$$\partial_t\tilde{\psi}_4 = \frac{1}{4F_A^2F_B^2}[(\sqrt{A^2+1}-1)^2\hat{\partial}_0\psi_0 + 4iA(\sqrt{A^2+1}-1)\hat{\partial}_0\psi_1 - 6A^2\hat{\partial}_0\psi_2 - 4iA(\sqrt{A^2+1}+1)\hat{\partial}_0\psi_3 + (\sqrt{A^2+1}+1)^2\hat{\partial}_0\psi_4].$$

(e) Use the $e^{im\phi_{KS}}$ decomposition which is affected by the φ transformation given in Eqs. (4.4) and (6.4). This transformation is implemented at the end of the calculation by $\tilde{\psi}_4 \to e^{im\varphi_{Shift}}\tilde{\psi}_4$ and likewise for $\partial_t\tilde{\psi}_4$. Note that the calculation of the last shift correction term in Eqs. (A22) can also be conveniently carried over after step (e) rather than in step (d).

[1] S.P. Zwart and S. McMillan, Astrophys. J. Lett. **528**, L17 (2000).
[2] S.P. Zwart and S. McMillan, Int. J. Mod. Phys. A **15**, 4871 (2000).
[3] R.H. Price and J. Pullin, Phys. Rev. Lett. **72**, 3297 (1994).
[4] M. Alcubierre, W. Benger, B. Brügmann, G. Lanfermann, L. Nerger, E. Seidel, and R. Takahashi, Phys. Rev. Lett. (to be published), gr-qc/0012079.
[5] J. Baker, B. Brügmann, M. Campanelli, and C.O. Lousto, Class. Quantum Grav. **17**, L149 (2000).
[6] J. Baker, B. Brügmann, M. Campanelli, C.O. Lousto, and R. Takahashi, Phys. Rev. Lett. **87**, 121103 (2001).
[7] A. Abrahams and R. Price, Phys. Rev. D **53**, 1963 (1996).
[8] A.M. Abrahams, S.L. Shapiro, and S.A. Teukolsky, Phys. Rev. D **51**, 4295 (1995).
[9] S.A. Teukolsky, Astrophys. J. **185**, 635 (1973).
[10] J. Baker and M. Campanelli, Phys. Rev. D **62**, 127501 (2000).
[11] G.B. Cook, Phys. Rev. D **50**, 5025 (1994).
[12] S. Brandt and B. Brügmann, Phys. Rev. Lett. **78**, 3606 (1997).
[13] T.W. Baumgarte, Phys. Rev. D **62**, 024018 (2000).

[14] L. Smarr and J. York, Phys. Rev. D **17**, 2529 (1978).
[15] D. Garfinkle and G.C. Duncan, Phys. Rev. D **63**, 044011 (2001).
[16] R. Arnowitt, S. Deser, and C. W. Misner, in *Gravitation: An Introduction to Current Research*, edited by L. Witten (Wiley, New York, 1962), pp. 227–265.
[17] M. Alcubierre, B. Brügmann, T. Dramlitsch, J. Font, P. Papadopoulos, E. Seidel, N. Stergioulas, W.-M. Suen, and R. Takahashi, Phys. Rev. D **62**, 044034 (2000).
[18] M. Alcubierre, S. Brandt, B. Brügmann, C. Gundlach, J. Massó, and P. Walker, Class. Quantum Grav. **17**, 2159 (2000).
[19] R.J. Gleiser, C.O. Nicasio, R.H. Price, and J. Pullin, Phys. Rev. Lett. **77**, 4483 (1996).
[20] P. Anninos, K. Camarda, J. Massó, E. Seidel, W.-M. Suen, and Phys. Rev. D **52**, 2059 (1995).
[21] M. Campanelli and C.O. Lousto, Phys. Rev. D **58**, 024015 (1998).
[22] M. Campanelli, W. Krivan, and C.O. Lousto, Phys. Rev. D **58**, 024016 (1998).
[23] M. Campanelli, C.O. Lousto, J. Baker, G. Khanna, and J. Pullin, Phys. Rev. D **58**, 084019 (1998); **62**, 069901(E) (2000).
[24] M. Campanelli and C.O. Lousto, Phys. Rev. D **59**, 124022 (1999).
[25] C.O. Lousto, Phys. Rev. D **63**, 047504 (2001).
[26] W. Krivan, P. Laguna, P. Papadopoulos, and N. Andersson, Phys. Rev. D **56**, 3395 (1997).
[27] M. Campanelli, G. Khanna, P. Laguna, J. Pullin, and M.P. Ryan, Class. Quantum Grav. **18**, 1543 (2001).
[28] http://www.cactuscode.org
[29] G. Khanna, R. Gleiser, R. Price, and J. Pullin, New J. Phys. **2**, 3 (2000).
[30] M. Alcubierre, B. Brügmann, D. Pollney, E. Seidel, and R. Takahashi (unpublished).
[31] J. Pullin (private communication).
[32] H.P. Pfeiffer, S.A. Teukolsky,, and G.B. Cook, Phys. Rev. D **62**, 104018 (2000).
[33] T. Damour, B.R. Iyer, and B.S. Sathyaprakash, Phys. Rev. D **63**, 044023 (2001).